

Article

Switchable Coupled Relays Aid Massive Non-Orthogonal Multiple Access Networks with Transmit Antenna Selection and Energy Harvesting

Thanh-Nam Tran ^{1,2,*}  and Miroslav Voznak ^{1,†} 

¹ Faculty of Electrical Engineering and Computer Science, VSB-Technical University of Ostrava, 17. Listopadu 2172/15, 708 00 Ostrava, Czech Republic; miroslav.voznak@vsb.cz

² Faculty of Electronics and Communications, Sai Gon University, 273 An Duong Vuong, Hochiminh 700 00, Vietnam

* Correspondence: thanh.nam.tran.st@vsb.cz

† These authors contributed equally to this work.

Abstract: The article proposes a new switchable coupled relay model for massive MIMO-NOMA networks. The model equips a much greater number of antennas on the coupled relays to dramatically improve capacity and Energy Efficiency (EE). Each relay in a coupled relay is selected and delivered into a single transmission block to serve multiple devices. This paper also plots a new diagram of two transmission blocks which illustrates energy harvesting and signal processing. To optimize the system performance of a massive MIMO-NOMA network, i.e., Outage Probability (OP) and system throughput, this paper deploys a Transmit Antenna Selection (TAS) protocol to select the best received signals from the pre-coding channel matrices. In addition, to achieve better EE, Simultaneously Wireless Information Power Transmit (SWIPT) is implemented. Specifically, this paper derives the novel theoretical analysis in closed-form expressions, i.e., OP, system throughput and EE from a massive MIMO-NOMA network aided by switchable coupled relays. The theoretical results obtained from the closed-form expressions show that a massive MIMO-NOMA network achieves better OP and greater capacity and expends less energy than the MIMO technique. Finally, independent Monte Carlo simulations verified the theoretical results.

Keywords: non-orthogonal multiple access; multiple devices; multiple antennas; massive MIMO; transmit antenna selection; energy harvesting



Citation: Tran, T.-N.; Voznak, M. Switchable Coupled Relays Aid Massive Non-Orthogonal Multiple Access Networks with Transmit Antenna Selection and Energy Harvesting. *Sensors* **2021**, *21*, 1101. <http://doi.org/10.3390/s21041101>

Academic Editor: Gianmarco Romano
Received: 14 December 2020
Accepted: 1 February 2021
Published: 5 February 2021

Publisher's Note: MDPI stays neutral with regard to jurisdictional claims in published maps and institutional affiliations.



Copyright: © 2021 by the authors. Licensee MDPI, Basel, Switzerland. This article is an open access article distributed under the terms and conditions of the Creative Commons Attribution (CC BY) license (<https://creativecommons.org/licenses/by/4.0/>).

1. Introduction

Relays are proven suitable solutions for extending networking coverage. In addition, Multiple-Input–Multiple-Output (MIMO) Non-Orthogonal Multiple Access (NOMA) technologies are effective methods for enhancing the capacity of fifth-generation (5G) wireless communication networks and beyond. The NOMA technique improves spectral sharing and the capability for a greater number of connections in the same time slot/frequency [1,2]. The NOMA technique in fifth-generation (5G) wireless communication networks and beyond could therefore serve large numbers of devices. The NOMA technique's feature is the ability to broadcast a superimposed signal to devices in the network with different Power Allocation (PA) factors [3]. The farthest device with poorest Channel State Information (CSI) is allocated the largest PA factor compared to other PA factors allocated to other devices. Successive Interference Cancellation (SIC) [4] implemented at the receiver device removes interference before the device decodes its own message in the superimposed signal by treating other device information which has a stronger PA factor [5]. Major studies have significantly contributed to NOMA through the application of new techniques in 5G networks and beyond. In [6], the authors verified that the system performance of NOMA networks is dependent on power resource allocation. The main aims of NOMA networks

are to serve more devices [7] and fairness in Quality of Service (QoS) [8]. In achieving these aims, previous studies verify that the system performance of NOMA wireless networks are significantly affected by power resource allocation strategies [9,10]. The authors verified that PA factors in NOMA networks could be allocated by device CSI and device data rate thresholds [11].

Recently, a cooperative networking solution has drawn much attention as an emerging method to extend network coverage. Specifically, in a cooperative NOMA network, a relay is deployed to receive and forward superimposed signals to the devices outside the network area. The radius of the network coverage is thus expanded, and its reliability is improved by enhancing QoS for devices [12]. Some major techniques may be fully deployed at the relay, namely Half-Duplex (HD), Full-Duplex (FD), Decode-and-Forward (DF), and Amplify-and-Forward (AF) [13]. Some studies have made significant contributions to cooperative NOMA [14,15]. These studies have shown that the system performance of NOMA wireless networks can be improved by deploying multiple relays in combination with the selection of the best relay in individual schemes [16–19].

In addition, to improve the capacity of a NOMA wireless network, the massive MIMO technique [20] is emerging as a good solution which extends the MIMO technique [21,22]. However, under this technique, networked devices equip more antennas, leading to increased costs for hardware and RF. The authors proposed the deployment of a TAS protocol which selects the best channel [23,24]. The authors also designed the pre-coding matrices for optimal system throughput in a multi-cell MIMO-NOMA network. However, massive NOMA has many research challenges which require careful investigation, such as extending the massive MIMO network which consider relaying and TAS and SWIPT protocols.

Another potential technology for future 5G networks and beyond is the simultaneous transmission of information with Radio Frequency (RF) and Energy Harvesting (EH) [25–31]. A study [26] on wireless EH offers a deep survey of the advantages of SWIPT. The authors surveyed several SWIPT technologies: SWIPT enabled multi-carrier systems, full-duplex SWIPT systems, etc. Given the explosion in the number of networked devices, for example Internet of Things (IoTs) devices, the energy issue is especially important. Time Switching (TS) [28] and Power Splitting (PS) [29–31] represent a solution for simultaneous data and energy transmission. Previous studies [28–31] which contained some problems requiring further investigation were the motivations which led to this study. In [28], the authors proposed a MIMO system consisting of a single transmitter which served a single receiver. The authors adopted the TS framework as in [28] (Figure 2), and the framework was split into two time slots. The first time slot was used for the transmission of wireless power [28] (Equation (3)), and the second time slot was used for the transmission of wireless information [28] (Equation (4)). However, the authors adopted PS frameworks for cooperative NOMA networks to assist the far device through a single relay equipped with a single antenna [29–31]. The authors deployed multiple relays to aid a single destination [31] (Figures 1a and 3a) by adopting TS and PS frameworks [31] (Figures 1b and 3b), respectively.

This study was inspired by the major studies [29,31]. The authors of [31] adopted a SWIPT protocol and depicted TS and PS frameworks fully. However, the system models in [31] were only designed to serve a single destination whereas the authors of [29] deployed a cooperative NOMA network to serve multiple devices (two devices). However, the author of [29] equipped a single antenna on each network node. The authors of the present study designed a network to serve a greater number of devices than the number of devices in [29,31] and improved networking capacity by equipping a greater number of antennas on network nodes, i.e., BS, coupled relays, and devices.

The study's main aims are also its major contributions:

- We present a new design for a switchable coupled relay model to assist massive MIMO-NOMA wireless networks. Each relay in a coupled relay is selected and delivered into odd/even transmission blocks. The selected relay is used to forward signals to multiple devices while another relay maintains EH.

- We present a new design for a diagram of two transmission blocks to calculate the propagation of wireless information and power (WIP). The present paper offers the potential for the practical application of wireless sensor networks (WSNs), e.g., in a water environment where relays and devices are barely powered [32].
- We maximize system throughput in a massive MIMO-NOMA network. The study deploys a TAS protocol which selects the best received signals from the pre-coding channel matrices.
- The study delivers novel expressions for OP, system throughput, and EE in closed-forms. We apply Monte Carlo simulation results to verify the analysis results.

This paper is structured as follows. Section 2 introduces system modeling. Section 3 presents an analysis of the system model. We describe and discuss the analysis and simulation results in Section 4. Section 5 presents a summary of the paper.

2. System Model

2.1. New Design for a Cooperative MIMO-NOMA Scheme

The present paper examines a new cooperative MIMO-NOMA model for emerging 5G wireless networks and networks beyond. Figure 1 depicts the system model containing a BS, coupled relay $\mathcal{R} = \{R_1, R_2\}$, and multiple devices $D_n = \{D_1, \dots, D_N\}$. To benefit a massive MIMO-NOMA network, the study equips a large number of antennas A_0 , A_1 , and A_2 at the network nodes and BS, coupled relays, and devices, respectively. In addition, we assume that the BS has full knowledge of the CSI [26,33]. As with the system models in the major studies [28–31], the massive MIMO underlay cooperative NOMA model shown in Figure 1 contains two time slots to complete a transmission block. It is important to illustrate the difference to previous major studies. In [16–19], the authors verified that relays are a good solution to assist in combating channel fading. In other major studies, the authors deployed a SISO relay to aid a multi-destinations [29] or a multiple SISO relay to aid a single destination [31]. The authors also proposed relay selection strategies to select the best nearest relay [17] and max-instantaneous data rate [18] (Equation (16)) to assist the destinations. The present study deploys coupled relays to assist massive MIMO-NOMA networks, however, only the relay with better power capacity among the coupled relays is selected for cooperating devices in an odd/even transmission block., i.e., while one relay is selected to forward the signal to devices, another relay has to maintain EH from the BS.

Note that the present study is designed to serve multiple devices simultaneously. The coupled relays must first have the device CSI and report this information to the BS. Based on the device CSI, the BS allocates PS factors, whereas the coupled relays feed back their own CSIs to the BS and other devices. Based on the energy capacity information, the BS selects the best powered relay to forward the signal. The devices then wait to receive the signal from the strongest powered relay. In the case of insufficient CSI, the BS may select the poorest powered relay to forward the signal, leading to a reduced lifespan of the relay. This may interrupt signal propagation because the devices are waiting for a non-cooperative relay.

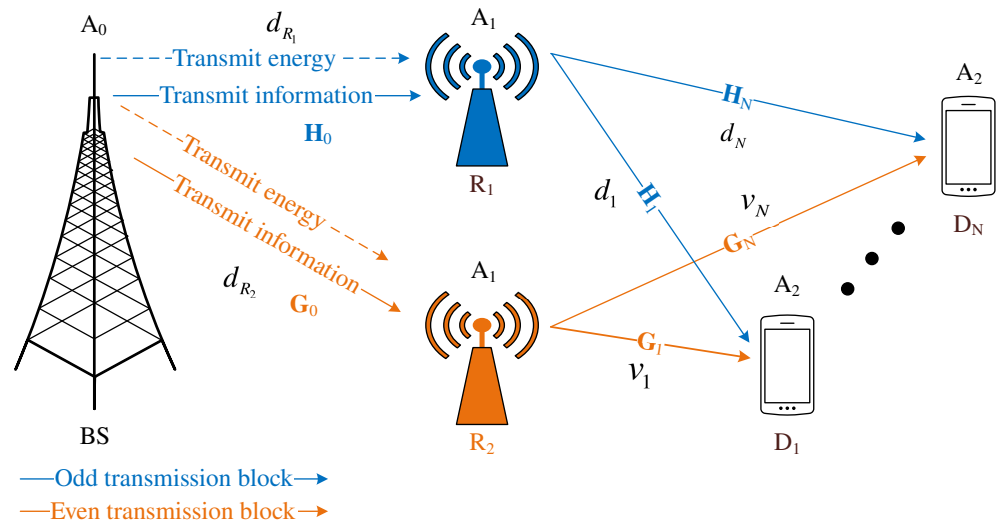


Figure 1. Coupled relays in a cooperative MIMO-NOMA network with the application of TAS and SWIPT.

2.2. Propagation and Formulations

From the model depicted in Figure 1, we designed a new propagation diagram, as shown in Figure 2. The coupled relays feed back data to the BS about their energy capacities. The BS decides which relay has more energy to forward the superimposed signal, while the remaining relay has less energy to maintain EH. Two main phases take place: EH and data transmission (DT). To illustrate, Figure 2 depicts two transmission blocks: an odd transmission block $T^{(odd)}$ and an even transmission block $T^{(even)}$. Each transmission block $T^{(\theta)}$ for $\theta = \{odd, even\}$ is separated into two equal time slots. The first time slot $T_1^{(odd)} = T^{(odd)} / 2$ in odd transmission block $T^{(odd)}$ is used by the BS to transmit wireless energy and superimposed information to coupled relays $\mathcal{R} = \{R_1, R_2\}$. In terms of the SWIPT technique with a PS protocol, during the first time slot $T_1^{(odd)}$, a fraction λ of the power domain P_S is used for EH while the remaining fraction $(1 - \lambda)$ of the power domain P_S is used to superimpose data from the BS. The second time slot $T_2^{(odd)} = T^{(odd)} / 2$ in odd transmission block $T^{(odd)}$ is used by the best powered relay to forward the superimposed signal to devices, while the worse powered relay applies EH from the BS, where the PS factor $\lambda = 1$. The present study assumes that relay R_1 is selected in the odd transmission block because relay R_1 has more energy than relay R_2 . Therefore, relay R_2 maintains EH from the BS. Similarly, the even transmission block $T^{(even)}$ is also separated into two equal time slots. The first time slot $T_1^{(even)} = T^{(even)} / 2$ in even transmission block $T^{(even)}$ is also used by the BS to simultaneously transmit wireless energy and the superimposed signal to the coupled relay $\mathcal{R} = \{R_1, R_2\}$. However, in the second time slot $T_2^{(even)} = T^{(even)} / 2$ in even transmission block $T^{(even)}$, the relay R_2 is selected to forward the superimposed signal to devices instead of relay R_1 because relay R_2 harvested energy from the BS, where $\lambda = 1$ during $T_2^{(odd)}$, and then relay R_2 contains more energy than relay R_1 . As a result, relay R_1 maintains EH from the BS with PS factor $\lambda = 1$ during $T_2^{(even)}$. Although the network model shown in Figure 1 is complex, it requires two time slots for signals to propagate through the network as in studies [28,29,31]. Specifically, the present study examines how multiple devices are served simultaneously. We therefore adopt the emerging NOMA technique. The BS also superimposes all the information of devices in the same signal by sharing the spectrum. The devices may be thus served simultaneously. As a result, the massive MIMO-NOMA network in the present study are low latency.

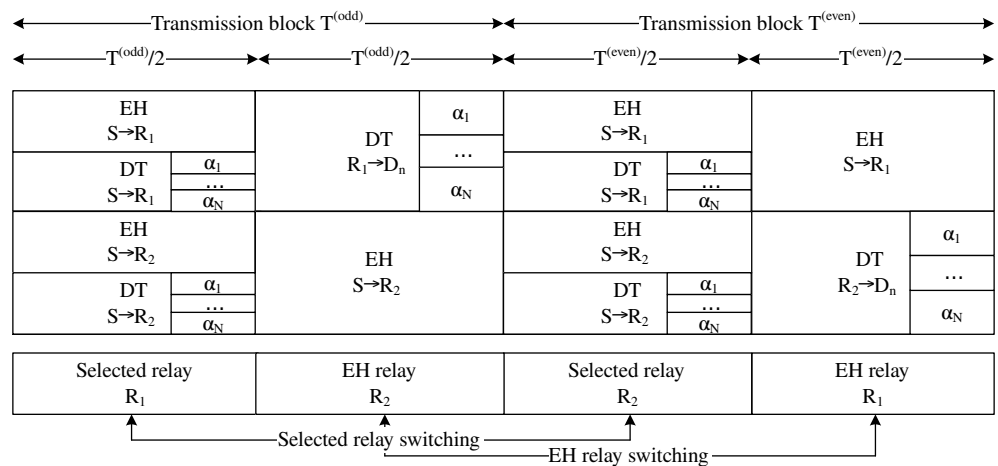


Figure 2. Diagram of two transmission blocks.

2.2.1. Odd Transmission Block

As shown in Figure 1, it is important to note that both the BS and coupled relays (R_1 and R_2) are equipped with multiple antennas, where $A_0 > 1$ and $A_1 > 1$. A_0 and A_1 are the number of antennas at the BS and coupled relays, respectively. Tran et al. [23] designed a pre-coding channel matrix size of [number of transmitting antennas \times number of receiving antennas]. We therefore designed the pre-coding channel matrices from the A_0 transmitting antennas at the BS to the A_1 receiving antennas on the coupled relays R_1 and R_2 , respectively, as follows:

$$\mathbf{H}_0 = \begin{bmatrix} h_0^{(1,1)} & \cdots & h_0^{(1,A_1)} \\ \vdots & \ddots & \vdots \\ h_0^{(A_0,1)} & \cdots & h_0^{(A_0,A_1)} \end{bmatrix}, \quad (1)$$

$$\mathbf{G}_0 = \begin{bmatrix} g_0^{(1,1)} & \cdots & g_0^{(1,A_1)} \\ \vdots & \ddots & \vdots \\ g_0^{(A_0,1)} & \cdots & g_0^{(A_0,A_1)} \end{bmatrix}, \quad (2)$$

where $h_0^{(a_0,a_1)} \in \mathbf{H}_0$ and $g_0^{(a_0,a_1)} \in \mathbf{G}_0$ for $a_0 \in A_0$ and $a_1 \in A_1$ are channels from a transmitting antenna a_0 at the BS to a receiving antenna a_1 at the coupled relays R_1 and R_2 . In addition, the fading channels are modeled over Rayleigh distributions with $h_0^{(\cdot)}$ and $g_0^{(\cdot)}$ following $h_0^{(\cdot)} = d_{R_1}^{-\omega}$ and $g_0^{(\cdot)} = d_{R_2}^{-\omega}$, where d_{R_1} and d_{R_2} are the distances from the BS to coupled relays R_1 and R_2 , respectively, and the coefficient ω is the path-loss exponent factor.

By applying the PS protocol, the first time slot in the odd transmission block $T_1^{(odd)}$ is used for the BS to transmit wireless energy and superimposed information simultaneously. To illustrate, two phases take place. In the first phase, the BS sends wireless energy to the coupled relay with the PS factor λ . Therefore, the EH from the best channel in the pre-coding channel matrices given by (1) and (2) in the first time slot $T_1^{(odd)}$ in odd transmission block $T^{(odd)}$ at coupled relays R_1 and R_2 are expressed as follows:

$$E_{R_1}^{(T_1^{(odd)})} = \eta \lambda P_S \max_{[A_0 \times A_1]} \{ |\mathbf{H}_0|^2 \}, \quad (3)$$

$$E_{R_2}^{(T_1^{(odd)})} = \eta \lambda P_S \max_{[A_0 \times A_1]} \{|\mathbf{G}_0|^2\}, \quad (4)$$

where η is the collection factor, λ is the PS factor, and P_S is the transmission power at the BS.

In the second phase of the first time slot $T_1^{(odd)}$ in odd transmission block $T^{(odd)}$, in a major advantage of NOMA theories, the BS broadcasts a superimposed signal by superimposing the messages x_i of devices D_i for $i = \{1, \dots, N\}$ to the coupled relays R_1 and R_2 . We assume that no direct down-link exists from the BS to the devices. The received signal at the coupled relays is expressed as follows:

$$\max_{[A_0 \times A_1]} \left\{ \mathbf{Y}_{R_1}^{(T_1^{(odd)})} \right\} = \sqrt{1 - \lambda} \max_{[A_0 \times A_1]} \{|\mathbf{H}_0|\} \sum_{i=N}^1 \sqrt{\alpha_i P_S} x_i + n_{R_1}, \quad (5)$$

$$\max_{[A_0 \times A_1]} \left\{ \mathbf{Y}_{R_2}^{(T_1^{(odd)})} \right\} = \sqrt{1 - \lambda} \max_{[A_0 \times A_1]} \{|\mathbf{G}_0|\} \sum_{i=N}^1 \sqrt{\alpha_i P_S} x_i + n_{R_2}, \quad (6)$$

where $n_{\mathcal{R}} \sim CN(0, N_0)$ is the Additive White Gaussian Noise (AWGN) at the coupled relays $\mathcal{R} = \{R_1, R_2\}$ with zero mean and variance N_0 . The PA factors for devices D_i for $i = \{N, \dots, 1\}$ are, respectively, denoted by α_i , constrained to $\alpha_1 < \dots < \alpha_N$, $\alpha_1 + \dots + \alpha_N = 1$, and given by

$$\alpha_i = i / \sum_{n=1}^N n. \quad (7)$$

Note that Expression (7) is derived from the feature studied [7]. However, the devices in [7] were ordered where D_1 is the farthest device. However, the system model shown Figure 1 indicates that device D_N has the farthest distance from the coupled relays. In term of NOMA theory, the farthest device must be allocated the biggest PA factor. As a result, the PA factor α_N for device D_N is the largest value among the PA factors, whereas device D_1 is the nearest distance from the coupled relays. Therefore, device D_1 is allocated the smallest PA factor.

SIC is another feature of NOMA theories which is implemented at the user. The user therefore implements SIC to detect messages in the received signal. In [7,12], the authors investigated NOMA networks with a random number N of users. The users repeated the SIC phases until their own messages were successfully detected in the received signal. It is important to note that N devices exist in our model (Figure 1), and, therefore, N SIC phases at the relay R_1 . After selecting the received signal as given in (5), in the first SIC phase, relay R_1 detects the message x_N of device D_N as a result of the constraint of the PA factors $\alpha_N > \dots > \alpha_1$. In the second SIC phase, relay R_1 detects the message x_{N-1} of device D_{N-1} after removing the x_N symbol from the received signals. The relay R_1 repeats SIC until it successfully detects the last symbol x_1 .

However, the present study examines a massive MIMO underlay cooperative NOMA network in contrast to the schemes presented in [29,31], where the author studied cooperative Single-Input-Single-Output (SISO)-NOMA schemes. Fortunately, the authors of [23,24] also investigated a MIMO-NOMA network with TAS and obtained Signal-to-Interference-plus-Noise Ratios (SINRs), where the devices detected information by applying SIC. To optimize system performance, our study considers the massive MIMO technique in combination with a TAS protocol, where relay R_1 selects the best received signal

$\max \left\{ \left| \mathbf{Y}_{R_1}^{(T_1^{(odd)})} \right| \right\}$ for SIC. In the first SIC phase, relay R_1 decodes the x_N symbol from the best received signal $\max \left\{ \left| \mathbf{Y}_{R_1}^{(T_1^{(odd)})} \right| \right\}$ by treating the data symbols $x_j = \{x_1, \dots, x_{N-1}\}$

and AWGN n_{R_1} as interference. The SINR is therefore obtained when relay R_1 decodes the x_i symbol, as follows:

$$\max_{[A_0 \times A_1]} \left\{ \gamma_{R_1-x_i}^{(T_1^{(odd)})} \right\} = \frac{(1-\lambda) \max_{[A_0 \times A_1]} \{ |\mathbf{H}_0|^2 \} \alpha_i \rho_S}{(1-\lambda) \max_{[A_0 \times A_1]} \{ |\mathbf{H}_0|^2 \} \rho_S \sum_{j=1}^{i-1} \alpha_j + 1}, \text{ for } i > 1, \quad (8)$$

$$= (1-\lambda) \max_{[A_0 \times A_1]} \{ |\mathbf{H}_0|^2 \} \alpha_i \rho_S, \quad \text{for } i = n = 1, \quad (9)$$

where ρ_S is the transmission Signal-to-Noise Ratio (SNR) and $\rho_0 = P_S/N_0$.

Maximization of the instantaneous bit rate threshold is achieved at relay R_1 when relay R_1 decodes the message x_i for $i = \{N, \dots, 1\}$ as follows:

$$\max_{[A_0 \times A_1]} \left\{ \mathbf{R}_{R_1-x_i}^{(T_1^{(odd)})} \right\} = \frac{1}{2} \log_2 \left(1 + \max_{[A_0 \times A_1]} \left\{ \gamma_{R_1-x_i}^{(T_1^{(odd)})} \right\} \right). \quad (10)$$

In the second time slot $T_2^{(odd)}$ in the odd transmission block $T^{(odd)}$, the relay R_1 retrieves the messages $x_i = \{x_N, \dots, x_1\}$ and forwards the messages to the devices in the superimposed signal while the relay R_2 continues harvesting energy from the BS. Therefore, the received signal at devices D_n for $n = \{1, \dots, N\}$ and the EH at relay R_2 are expressed, respectively, as follows:

$$\max_{[A_1 \times A_2]} \left\{ \mathbf{Y}_{n \in N}^{(T_2^{(odd)})} \right\} = \max_{[A_1 \times A_2]} \{ |\mathbf{H}_n| \} \sum_{i=N}^1 \sqrt{\alpha_i P_{R_1}} x_i + n_n, \quad (11)$$

$$E_{R_2}^{(T_2^{(odd)})} = \eta \lambda P_S \max_{[A_0 \times A_1]} \{ |\mathbf{G}_0|^2 \}, \quad (12)$$

where P_{R_1} is the transmission power at relay R_1 and $n_n \sim CN(0, N_0)$ is the AWGN at device D_n for $n = \{1, \dots, N\}$ which follows zero mean and variance N_0 .

Note that the pre-coding channel matrix \mathbf{H}_n is given by

$$\mathbf{H}_n = \begin{bmatrix} h_n^{(1,1)} & \dots & h_n^{(1,A_2)} \\ \vdots & \ddots & \vdots \\ h_n^{(A_1,1)} & \dots & h_n^{(A_1,A_2)} \end{bmatrix}, \quad (13)$$

where the channel $h_n^{(a_1, a_2)}$ in the pre-coding channel matrix \mathbf{H}_n , where $a_1 \in A_1$ and $a_2 \in A_2$, is a channel from transmitting antenna a_1 at relay R_1 to a receiving antenna a_2 at a device D_n , also applying Rayleigh distribution for propagation. Each fading channel gain is given by $h_n^{(r)} = d_n^{-\omega}$, where d_n is the distance from relay R_1 to device D_n .

As a result of the combination of TAS and SIC, the SINRs are obtained at devices D_n for $n = \{1, \dots, N\}$ when the devices decode data symbols x_i for $i = \{N, \dots, n\}$ from the best received signal $\max \{ |\mathbf{Y}_2| \}_{A_1 \times A_2}$ by treating the data symbols x_j for $j = \{1, \dots, i-1\}$ and AWGN n_n as interference:

$$\max_{[A_1 \times A_2]} \left\{ \gamma_{n \in N}^{(T_2^{(odd)})} \right\}_{i=\{N, \dots, n\}}^{x_i} = \frac{\max_{[A_1 \times A_2]} \left\{ |\mathbf{H}_n|^2 \right\} \alpha_i \rho_{R_1}}{\max_{[A_1 \times A_2]} \left\{ |\mathbf{H}_n|^2 \right\} \sum_{j=1}^{i-1} \alpha_j \rho_{R_1} + 1}, \text{ for } i > 1, \quad (14)$$

$$= \max_{[A_1 \times A_2]} \left\{ |\mathbf{H}_n|^2 \right\} \alpha_i \rho_{R_1}, \quad \text{for } i = n = 1, \quad (15)$$

where SNR $\rho_{R_1} = P_{R_1}/N_0$.

The achievable bit-rate reached at device D_n when it decodes the data symbol x_i for $i = \{N, \dots, n\}$ from the best received signal $\max\{|\mathbf{Y}_n|\}$ is expressed as follows:

$$\max_{[A_1 \times A_2]} \left\{ \mathbf{R}_{n \in N}^{(T_2^{(odd)})} \right\}_{i=\{N, \dots, n\}}^{x_i} = \frac{1}{2} \log_2 \left(1 + \max_{[A_1 \times A_2]} \left\{ \gamma_{n \in N}^{(T_2^{(odd)})} \right\}_{i=\{N, \dots, n\}}^{x_i} \right). \quad (16)$$

2.2.2. Even Transmission Block

As with the first time slot in the odd transmission block, by applying the PS protocol, the first time slot in the even transmission block $T_1^{(even)}$ is used by the BS to transmit wireless energy and superimposed information simultaneously to coupled relays. The EH from the best channel in the pre-coding channel matrix at coupled relays R_1 and R_2 is expressed as follows:

$$E_{R_1}^{T_1^{(even)}} = \eta \lambda P_S \max_{[A_0 \times A_1]} \left\{ |\mathbf{H}_0|^2 \right\}, \quad (17)$$

$$E_{R_2}^{T_1^{(even)}} = \eta \lambda P_S \max_{[A_0 \times A_1]} \left\{ |\mathbf{G}_0|^2 \right\}, \quad (18)$$

where $T_1^{(odd)} = T^{(odd)}/2$.

The BS broadcasts a superimposed signal by combining the independent messages x_i of devices D_i for $i = \{N, \dots, 1\}$. Therefore, the received signal at coupled relays is expressed as follows:

$$\max_{[A_0 \times A_1]} \left\{ \mathbf{Y}_{R_1}^{(T_1^{(even)})} \right\} = \sqrt{1-\lambda} \max_{[A_0 \times A_1]} \left\{ |\mathbf{H}_0| \right\} \sum_{i=N}^1 \sqrt{\alpha_i P_S} x_i + n_{R_1}, \quad (19)$$

$$\max_{[A_0 \times A_1]} \left\{ \mathbf{Y}_{R_2}^{(T_1^{(even)})} \right\} = \sqrt{1-\lambda} \max_{[A_0 \times A_1]} \left\{ |\mathbf{G}_0| \right\} \sum_{i=N}^1 \sqrt{\alpha_i P_S} x_i + n_{R_2}. \quad (20)$$

In the second transmission block, SIC is implemented at the relay R_2 . As with the SIC in the odd transmission block, the relay R_2 has to repeat SIC until it detect all data symbols x_i for $i = \{N, \dots, 1\}$ in the best received signal as (20). The SINRs are obtained when relay R_2 decodes the data symbols $x_i = \{x_N, \dots, x_1\}$ as follows:

$$\max_{[A_0 \times A_1]} \left\{ \gamma_{i=\{N, \dots, 1\}}^{(T_1^{(even)})} \right\}_{R_2-x_i} = \frac{(1-\lambda) \max_{[A_0 \times A_1]} \left\{ |\mathbf{G}_0|^2 \right\} \alpha_i \rho_S}{(1-\lambda) \max_{[A_0 \times A_1]} \left\{ |\mathbf{G}_0|^2 \right\} \rho_S \sum_{j=1}^{i-1} \alpha_j + 1}, \text{ for } i > 1, \quad (21)$$

$$= (1-\lambda) \max_{[A_0 \times A_1]} \left\{ |\mathbf{G}_0|^2 \right\} \alpha_i \rho_S, \quad \text{for } i = n = 1. \quad (22)$$

Similar to (8) and (8), maximization of the instantaneous bit-rate threshold achieved at the relay R_2 when the relay R_2 decodes data symbols x_i , where $i = \{N, \dots, 1\}$ is expressed as follows:

$$\max_{[A_0 \times A_1]} \left\{ \mathbf{R}_{R_2-x_i}^{(T_1^{(even)})} \right\} = \frac{1}{2} \log_2 \left(1 + \max_{[A_0 \times A_1]} \left\{ \gamma_{R_2-x_i}^{(T_1^{(even)})} \right\} \right). \quad (23)$$

By applying a DF protocol, relay R_2 recovers the decoded data symbols x_i for $i = \{N, \dots, 1\}$ and forwards a beamforming superimposed signal to devices D_n for $n = \{1, \dots, N\}$. The received signals in the second time slot $T_2^{(even)}$ in even transmission block $T^{(even)}$ at devices D_n while EH at relay R_1 are expressed, respectively, as follows:

$$\max_{[A_1 \times A_2]} \left\{ \mathbf{Y}_{n \in N}^{(T_2^{(even)})} \right\} = \max_{[A_1 \times A_2]} \{ |\mathbf{G}_n| \} \sum_{i=N}^1 \sqrt{\alpha_i P_{R_2} x_i + n_n}, \quad (24)$$

$$E_{R_1}^{(T_2^{(even)})} = \eta \lambda P_S \max_{[A_0 \times A_1]} \{ |\mathbf{H}_0|^2 \}, \quad (25)$$

where P_{R_2} is the transmission power at relay R_2 and the pre-coding channel matrix \mathbf{G}_n is given by

$$\mathbf{G}_n = \begin{bmatrix} g_n^{(1,1)} & \dots & g_n^{(1,A_2)} \\ \vdots & \ddots & \vdots \\ g_n^{(A_1,1)} & \dots & g_n^{(A_1,A_2)} \end{bmatrix} \quad (26)$$

where the channel $g_n^{(a_1, a_2)}$ in the pre-coding matrix channel \mathbf{G}_n , with $a_1 \in \mathcal{A}_1$ and $a_2 \in \mathcal{A}_2$, is a channel from transmitting antenna a_1 at relay R_2 to a receiving antenna a_2 at a device D_n , applying Rayleigh distributions for propagation. Each fading channel is represented by $g_n^{(\dots)}$ such that $g_n^{(\dots)} = v_n^{-\omega}$, where v_n is the distance from relay R_2 to device D_n .

The SINRs obtained at devices D_n for $n = \{1, \dots, N\}$ when they decode the data symbols x_i for $i = \{N, \dots, n\}$ from the best received signal $\max_{[A_1 \times A_2]} \left\{ \left| \mathbf{Y}_n^{(T_2^{(even)})} \right| \right\}$ are expressed as follows:

$$\max_{[A_1 \times A_2]} \left\{ \gamma_{n \in N - x_i}^{(T_2^{(even)})} \right\} = \frac{\max_{[A_1 \times A_2]} \{ |\mathbf{G}_n|^2 \} \alpha_i \rho_{R_2}}{\max_{[A_1 \times A_2]} \{ |\mathbf{G}_n|^2 \} \sum_{j=1}^{i-1} \alpha_j \rho_{R_2} + 1}, \quad \text{for } i > 1, \quad (27)$$

$$= \max_{[A_1 \times A_2]} \{ |\mathbf{G}_n|^2 \} \alpha_i \rho_{R_2}, \quad \text{for } i = n = 1, \quad (28)$$

where SNR $\rho_{R_2} = P_{R_2}/N_0$.

Maximization of the achievable bit-rate thresholds achieved at devices D_n when they decode the data symbols x_i for $i = \{N, \dots, n\}$ from the best received signal

$\max_{[A_1 \times A_2]} \left\{ \left| \mathbf{Y}_n^{(T_2^{(even)})} \right| \right\}$ is expressed as follows:

$$\max_{[A_1 \times A_2]} \left\{ \mathbf{R}_{n \in N - x_i}^{(T_2^{(odd)})} \right\} = \frac{1}{2} \log_2 \left(1 + \max_{[A_1 \times A_2]} \left\{ \gamma_{n \in N - x_i}^{(T_2^{(odd)})} \right\} \right). \quad (29)$$

3. System Performance Analysis

Many factors affect the system performance of wireless networks. The authors of [34] investigated the causes of OP at the BS, such as brief BS power supply variation, preventive BS activity state transition due to excessive temperature increase or decrease inside the BS rack, auto-recovery software and hardware failure, and temporal cell interference and congestion. The downlink MIMO-NOMA model with superposition transmission at BS and SIC at the terminal devices and the SIC processing is adopted in receiver side [35]. Therefore, our study considered OP at the receivers when the receivers could not successfully decode messages in the received signals. We analyze the system performance of the network model depicted in Figure 1 and delivers novel closed-forms of OP, system throughput and EE expressions at coupled relays $\mathcal{R} = \{R_1, R_2\}$ and devices D_n for $n = \{1, \dots, N\}$.

3.1. Outage Probability at the Coupled Relays \mathcal{R}

Theorem 1. *The outage event at a relay in the coupled relays \mathcal{R} occurs when the relay cannot successfully decode at least a data symbol $x_i \in \{x_N, \dots, x_1\}$ from the best received signal*

$\max_{[A_1 \times A_2]} \left\{ \left| \mathbf{Y}_{R_1}^{(T_2^{(odd)})} \right| \right\}$ for an odd transmission block or $\max_{[A_1 \times A_2]} \left\{ \left| \mathbf{Y}_{R_2}^{(T_2^{(even)})} \right| \right\}$ for an even transmission block, which is the best signal after TAS. Therefore, the coupled relays \mathcal{R} receive the best

superimposed signal $\max_{[A_1 \times A_2]} \left\{ \left| \mathbf{Y}_{\mathcal{R}}^{(T_2^{(\theta)})} \right| \right\}$ by applying a TAS protocol to select the best signal from the pre-coding channel matrix \mathbf{H}_0 for an odd transmission block or \mathbf{G}_0 for an even transmission block to maximize the SINRs $\gamma_{\mathcal{R}-x_i}^{(T_1^{(\theta)})}$, as given by (8), (9), (21), and (21), and maximize the instantaneous bit-rate threshold

$\max_{[A_0 \times A_1]} \left\{ \mathbf{R}_{\mathcal{R}-x_i}^{(T_1^{(\theta)})} \right\}_{i=\{N, \dots, 1\}}$, as given by (10) or (23). Maximization of

the instantaneous bit rate threshold $\max_{[A_0 \times A_1]} \left\{ \mathbf{R}_{\mathcal{R}-x_i}^{(T_1^{(\theta)})} \right\}_{i=\{N, \dots, 1\}}$ is then compared to a device's predefined

bit-rate threshold R_i^* , where $i = \{N, \dots, 1\}$. If maximization of the instantaneous bit-rate threshold

$\max_{[A_0 \times A_1]} \left\{ \mathbf{R}_{\mathcal{R}-x_i}^{(T_1^{(\theta)})} \right\}_{i=\{N, \dots, 1\}}$ is less than a device's predefined bit-rate threshold R_i^* , an outage event will

occur, i.e., the OP at coupled relays \mathcal{R} is expressed as follows:

$$\begin{aligned}
 OP_{\mathcal{R}}^{(T_1^{(\theta)})} &= \Pr \left\{ \max_{[A_0 \times A_1]} \left\{ \mathbf{R}_{\mathcal{R}-x_N}^{(T_1^{(\theta)})} \right\} < R_N^* \right\} \\
 &+ \Pr \left\{ \max_{[A_0 \times A_1]} \left\{ \mathbf{R}_{\mathcal{R}-x_N}^{(T_1^{(\theta)})} \right\} \geq R_N^*, \max_{[A_0 \times A_1]} \left\{ \mathbf{R}_{\mathcal{R}-x_{N-1}}^{(T_1^{(\theta)})} \right\} < R_{N-1}^* \right\} \\
 &+ \\
 &\vdots \\
 &+ \Pr \left\{ \max_{[A_0 \times A_1]} \left\{ \mathbf{R}_{\mathcal{R}-x_N}^{(T_1^{(\theta)})} \right\} \geq R_N^*, \max_{[A_0 \times A_1]} \left\{ \mathbf{R}_{\mathcal{R}-x_{N-1}}^{(T_1^{(\theta)})} \right\} \geq R_{N-1}^*, \dots, \right. \\
 &\left. \max_{[A_0 \times A_1]} \left\{ \mathbf{R}_{\mathcal{R}-x_2}^{(T_1^{(\theta)})} \right\} \geq R_2^*, \max_{[A_0 \times A_1]} \left\{ \mathbf{R}_{\mathcal{R}-x_1}^{(T_1^{(\theta)})} \right\} < R_1^* \right\}
 \end{aligned} \tag{30}$$

We obtain the OP at coupled relays $\mathcal{R} = \{R_1, R_2\}$ in novel closed-form as follows:

$$OP_{\mathcal{R}}^{(T_1^{(\theta)})} = \sum_{i=N}^1 \left(\prod_{a_0=0}^{A_0} \prod_{a_1=1}^{A_1} \left(1 - \exp \left(-\frac{\gamma_i^*}{(1-\lambda)\beta_i \rho_S \sigma_{\mathcal{R}}^2} \right) \right) \right. \\ \left. \times \prod_{k=N}^{i+1} \left(1 - \prod_{a_0=1}^{A_1} \prod_{a_1=1}^{A_1} \left(1 - \exp \left(-\frac{\gamma_k^*}{(1-\lambda) \left(\alpha_k - \gamma_k^* \sum_{j=1}^{k-1} \alpha_j \right) \rho_S \sigma_{\mathcal{R}}^2} \right) \right) \right) \right)_{\text{for } i < N}, \quad (31)$$

where β_i is given by

$$\beta_i = \alpha_i - \gamma_i^* \sum_{j=1}^{i-1} \alpha_j, \quad \text{for } i > 1, \quad (32)$$

$$\beta_i = \alpha_i, \quad \text{for } i = 1. \quad (33)$$

See Appendix A for proof.

Remark 1. If the network has a large number of devices, it is challenge to apply the expression (30) in Monte Carlo simulations. Fortunately, the authors of [12] analyzed a network model with multiple relays and multiple devices. The authors presented the expressions for OP at the relays as [12] (Equation (33)). It is important to mention that the present paper extends the work of the previous study [12] by deploying massive MIMO and TAS techniques. From [12] (Equation (33)), the OP expression at the coupled relay \mathcal{R} in (30) can be rewritten as follows:

$$OP_{\mathcal{R}}^{(T_1^{(\theta)})} = 1 - \prod_{i=N}^1 \Pr \left\{ \underbrace{\max \left\{ \mathbf{R}_{\mathcal{R}-x_i}^{(T_1^{(\theta)})} \right\}}_{Q_i} \geq R_i^* \right\}. \quad (34)$$

From (34), we obtain a novel expression of OP at the coupled relay \mathcal{R} in closed-form by applying the Cumulative Density Function (CDF) as defined in [13] (Equation (71)):

$$OP_{\mathcal{R}}^{(T_1^{(\theta)})} = 1 - \prod_{i=N}^1 \left(1 - \sum_{\psi=0}^{A_0 A_1} \frac{(-1)^\psi (A_0 A_1)!}{\psi! (A_0 A_1 - \psi)!} \exp \left(-\frac{\psi \gamma_i^*}{(1-\lambda)\beta_i \rho_S \sigma_{\mathcal{R}}^2} \right) \right). \quad (35)$$

See Appendix B for proof.

3.2. Outage Probability at Devices

Theorem 2. The outage event in an odd or even transmission block at devices D_n for $n = \{1, \dots, N\}$ occurs when, on the one hand, the relays R_1 and R_2 for odd and even transmission blocks, respectively, cannot successfully decode at least data symbol x_i for $i = \{N, \dots, n\}$ from the best received signal $\max_{[A_0 \times A_1]} \left\{ \left| \mathbf{Y}_{R_1}^{(T_1^{(odd)})} \right| \right\}$ as (5) or $\max_{[A_0 \times A_1]} \left\{ \left| \mathbf{Y}_{R_2}^{(T_1^{(even)})} \right| \right\}$ as (20). On the other hand, the coupled relays can successfully decode all data symbol x_i for $i = \{N, \dots, n\}$, but device D_n cannot successfully decode at least data symbols x_i for $i = \{N, \dots, n\}$ from the best received signal $\max_{[A_1 \times A_2]} \left\{ \left| \mathbf{Y}_n^{(T_2^{(odd)})} \right| \right\}$ as (11) for an odd transmission block or $\max_{[A_1 \times A_2]} \left\{ \left| \mathbf{Y}_n^{(T_2^{(even)})} \right| \right\}$ as (24) for an even transmission block.

Therefore, the OP at devices in an odd or even transmission block is expressed as follows:

$$\begin{aligned}
 OP_n^{(\theta)} = & \sum_{i=N}^n \left\{ \Pr \left\{ \max_{[A_0 \times A_1]} \left\{ \mathbf{R}_{\mathcal{R}-x_i}^{(T_1^{(\theta)})} \right\} < R_i^* \right\} \prod_{k=N}^{i+1} \underbrace{\Pr \left\{ \max_{[A_0 \times A_1]} \left\{ \mathbf{R}_{\mathcal{R}-x_k}^{(T_1^{(\theta)})} \right\} \geq R_k^* \right\}}_{\text{for } i < N} \right\} \\
 & + \sum_{i=N}^n \left\{ \Pr \left\{ \max_{[A_1 \times A_2]} \left\{ \mathbf{R}_{\mathcal{R}-x_i}^{(T_2^{(\theta)})} \right\} < R_i^* \right\} \prod_{k=N}^{i+1} \underbrace{\Pr \left\{ \max_{[A_1 \times A_2]} \left\{ \mathbf{R}_{\mathcal{R}-x_k}^{(T_2^{(\theta)})} \right\} \geq R_k^* \right\}}_{\text{for } i < N} \right\} \\
 & \times \prod_{t=N}^n \Pr \left\{ \max_{[A_0 \times A_1]} \left\{ \mathbf{R}_{\mathcal{R}-x_t}^{(T_1^{(\theta)})} \right\} \geq R_t^* \right\} \right\} \quad (36)
 \end{aligned}$$

From (36), the OP at user D_n is obtained in closed-form as follows:

$$\begin{aligned}
 OP_{n \in N}^{(\theta)} = & \sum_{i=N}^n \left(\underbrace{\prod_{a_0}^{A_0} \prod_{a_1}^{A_1} \left(1 - \exp \left(-\frac{\gamma_i^*}{(1-\lambda)\beta_i \rho_S \sigma_{\mathcal{R}}^2} \right) \right)}_{Q_i} \prod_{k=N}^{i+1} \underbrace{(1 - Q_k)}_{\text{for } i < N} \right) \\
 & + \sum_{i=N}^n \left(\underbrace{\prod_{a_1}^{A_1} \prod_{a_2}^{A_2} \left(1 - \exp \left(-\frac{\gamma_i^*}{\beta_i \rho_{\mathcal{R}} \sigma_n^2} \right) \right)}_{K_i} \prod_{k=N}^{i+1} \underbrace{(1 - K_k)}_{\text{for } i < N} \prod_{t=N}^n (1 - Q_t) \right) \quad (37)
 \end{aligned}$$

where $\sigma_n^2 = E\{|\mathbf{H}_n|^2\}$. Note that $\theta = \text{odd}$ and $\mathcal{R} = R_1$, or $\theta = \text{even}$ and $\mathcal{R} = R_2$.

See Appendix C for proof.

Similar to (30), note that Expression (36) is challenging in Monte Carlo simulations if the network has a large number of devices. Therefore, the OP at devices D_n can be rewritten as follows:

$$OP_n^{(\theta)} = 1 - \prod_{i=N}^n \Pr \left\{ \max_{[A_0 \times A_1]} \left\{ \mathbf{R}_{\mathcal{R}-x_i}^{(T_1^{(\theta)})} \right\} \geq R_i, \max_{[A_1 \times A_2]} \left\{ \mathbf{R}_{\mathcal{R}-x_i}^{(T_2^{(\theta)})} \right\} \geq R_i \right\}. \quad (38)$$

From (38), we obtain the expression of OP at devices D_n in closed-form as follows:

$$\begin{aligned}
 OP_n^{(\theta)} = & 1 - \prod_{i=N}^n \left(\left(1 - \sum_{\psi=0}^{A_0 A_1} \frac{(-1)^\psi (A_0 A_1)!}{\psi! (A_0 A_1 - \psi)!} \exp \left(-\frac{\psi \gamma_i^*}{(1-\lambda)\beta_i \rho_S \sigma_{\mathcal{R}}^2} \right) \right) \right. \\
 & \left. \times \left(1 - \sum_{\mu=0}^{A_1 A_2} \frac{(-1)^\mu (A_1 A_2)!}{\mu! (A_1 A_2 - \mu)!} \exp \left(-\frac{\mu \gamma_i^*}{\beta_i \rho_{\mathcal{R}} \sigma_n^2} \right) \right) \right). \quad (39)
 \end{aligned}$$

See Appendix D for the proof.

3.3. System Throughput

In Figures 1 and 2, the individual system model has two transmission blocks. Each odd or even transmission block is separated into two time slots. The achievable system throughput in an odd or even transmission block is the sum of the minimal device throughput at

the relay and device in the same transmission block. Therefore, the system throughput is expressed as follows:

$$TP^{(\theta)} = \sum_{n=1}^N \left(1 - \max \left\{ OP_{\mathcal{R}-x_n}^{(T_1^{(\theta)})}, OP_{n-x_n}^{(T_2^{(\theta)})} \right\} \right) R_n^* \quad (40)$$

3.4. Energy Efficiency

Green wireless networks require a higher throughput yet use lower energy. To achieve this aim, the present study deploys a massive MIMO technique and SWIPT protocol. As a result, the EE performance indicates the sum of device throughput and sum of transmission power at the BS and coupled relay ratio in the same transmission block. Therefore, the EE performance of an individual network model as given by Figure 1 is expressed as follows:

$$EE^{(\theta)} = \frac{\sum_{n=1}^N \left(1 - \max \left\{ OP_{\mathcal{R}-x_n}^{(T_1^{(\theta)})}, OP_{n-x_n}^{(T_2^{(\theta)})} \right\} \right) R_n^*}{(1 - \lambda)\rho_S + \rho_R}. \quad (41)$$

4. Numerical Results and Discussion

To investigate the system performance of the massive MIMO-NOMA network model shown in Figure 1, we propose parameters for both a theoretical analysis and the Monte Carlo simulations, as shown in Table 1.

Let a wireless network contain coupled relays and three devices ($N = 3$). The coupled relays are allocated nearby. The distances from the BS to the coupled relays are $d_{R_1} = d_{R_2} = 10$ m, and the distances from the coupled relays to devices D_1 , D_2 and D_3 are $d_1 = v_1 = 5$ m, $d_2 = v_2 = 7$ m and $d_3 = v_3 = 10$ m, respectively. The path-loss exponent refers to an indoor environment with $\lambda = 4$. By modeling the more challenging indoor environment, the performance bound of the less challenging outdoor scenario is therefore also covered. In 4G Long-Term Evolution (LTE) release 8, the maximum numbers of antennas at the BS and user equipment are 4T4R and 1T2R, respectively. In 4G LTE-Advanced (LTE-A), the number of antennas is greater to allow the use of 8T8R at BSs and 2T2R at devices in LTE-A schemes. Therefore, massive MIMO networks need at least an 8T8R antenna array at the BS. However, the present study assumes a certain number of antennas equipped at the BS ($A_0 = 4$), coupled relays R_1 ($A_1 = 4$), R_2 ($A_1 = 16$), and devices ($A_2 = 2$) to prove the benefits of massive MIMO (even transmission block) over MIMO (odd transmission block). The fading channel from the transmitting antennas at the BS to the receiving antennas at the coupled relays are distributed over Rayleigh fading channels. Based on distances and the path-loss exponent, the expected channel gains from the BS to coupled relays are $\sigma_{R_1}^2 = \sigma_{R_2}^2 = 1 \times 10^{-4}$ and from the coupled relays to devices D_1 , D_2 , and D_3 are $\sigma_1^2 = 16 \times 10^{-4}$, $\sigma_2^2 = 4.1649 \times 10^{-4}$, and $\sigma_3^2 = 1 \times 10^{-4}$. Each fading channel randomly generates 1e6 experiments. To simplify, the devices require the same bit-rate thresholds $R_1^* = R_2^* = R_3^* = 0.1 \text{bps/Hz}$ and SNR $\rho_S = \rho_R = \{0, \dots, 30\}$ dB. By applying (7), the PA factors for devices D_1 , D_2 , and D_3 are $\alpha_1 = 0.1667$, $\alpha_2 = 0.3333$, and $\alpha_3 = 0.5$, respectively. The present study assumes that coupled relays may fully collect EH ($\eta = 1$). The PS factor in an odd transmission block is $\lambda = 0.4$. Therefore, $0.4P_S$ and $0.6P_S$ are applied to EH and DT processing, respectively, whereas the PS factor in an even transmission block is reduced ($\lambda = 0.4$) since the relay R_2 in this block is equipped with a greater number of antennas than relay R_1 in an odd transmission block.

Table 1. Table of parameters.

Variables	Values	Units
N	3	
$d_{R_1} = d_{R_2}$	10	metres
$d_1 = v_1$	5	metres
$d_2 = v_2$	7	metres
$d_3 = v_3$	10	metres
α_1	0.1667	
α_2	0.3333	
α_3	0.5	
ω	4	
$\sigma_{R_1}^2 = \sigma_{R_2}^2$	1×10^{-4}	
σ_1^2	16×10^{-4}	
σ_2^2	4.1649×10^{-4}	
σ_3^2	1×10^{-4}	
$R_1^* = R_2^* = R_3^*$	0.1	bps/Hz
$\rho_S = \rho_{R_1} = \rho_{R_2}$	$\{0, \dots, 30\}$	dB
η	1	
A_0	4	
A_2	2	
	Odd transmission block	
A_1	4	
λ	0.4	
	Even transmission block	
A_1	16	
λ	0.6	

Figure 3 plots the OP performance at relay R_1 and devices in odd transmission blocks. Note the various markers and line plot analysis (Ana) and simulation (Sim) results. The analysis results of OP performance at relay R_1 are given by (30) or (34) and for devices D_n by (36) or (38). The analysis results were verified with Monte Carlo simulations for relay R_1 given by (31) or (35) and for devices by (37) or (39), where $\mathcal{R} = R_1$ and $\theta = odd$. Figure 3 illustrates that device D_3 achieved the best OP results, even though device D_3 was the farthest device and therefore allocated the biggest PA factor $\alpha_3 = 0.5$. When $\text{SRN} \rho \rightarrow \infty$, the OP results of relay R_1 and devices tend toward zero.

Figure 4 plots the OP performance at relay R_2 and devices in even transmission blocks. To improve the networking capacity and energy, we equipped a large number of antennas at relay R_2 and increased the PS factor $\lambda = 0.6$. By increasing the PS factor, relay R_1 was able to harvest more energy but relay R_2 could receive weak signals. However, we may observe that the OP performance at relay R_2 and devices in even transmission blocks (Figure 4) achieved better results than OP performance at relay R_1 and devices in odd transmission blocks (Figure 3). The analysis results of OP performance for relay R_2 are given by (30) or (34) and for devices D_n by (36) or (38), where $\mathcal{R} = R_2$ and $\theta = even$. The analysis results were verified with Monte Carlo simulations for relay R_2 given by (31) or (35) and for devices by (37) or (39), where $\mathcal{R} = R_2$ and $\theta = even$.

We may observe that the OP performances at relay R_2 and devices in even transmission blocks outperform those at relay R_1 and devices in odd transmission blocks at high SNRs such as $\rho_S = \rho_{\mathcal{R}} = 20$ dB. The present study thus exploits the advantages of a massive MIMO-NOMA network compared to a MIMO-NOMA network. We equipped a greater number of antennas on relay R_2 ($A_1 = 16$) than on relay R_1 ($A_1 = 4$). As a result, we obtained the respective pre-coding channel matrix sizes of $[4 \times 16]$ and $[16 \times 2]$ for \mathbf{G}_0 and \mathbf{G}_n , which, in the even transmission blocks, were much larger than the pre-coding channel matrix sizes of $[4 \times 4]$ and $[4 \times 2]$ for \mathbf{H}_0 and \mathbf{H}_n in odd transmission blocks. From Expressions (8), (9), (14), (15), (21), (22), (27), and (28) and by applying the TAS protocol, only the best channels from the pre-coding channel matrices are selected for data

decoding. Therefore, the relay R_2 and devices in even transmission blocks have better OP performance than relay R_1 and devices in odd transmission blocks under the same simulation parameters.

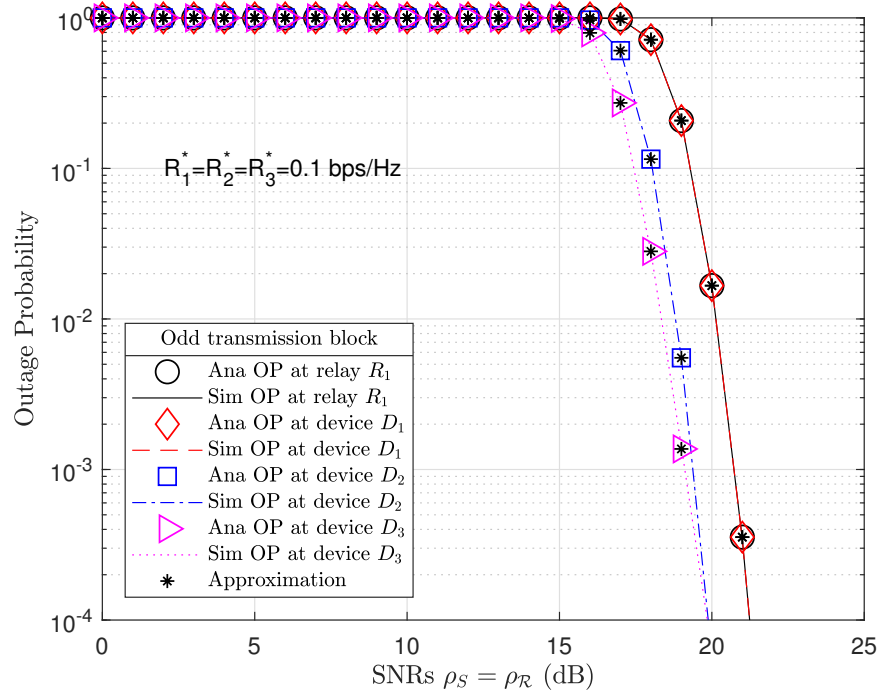


Figure 3. OP at relay R_1 and devices D_n for $n = \{1, \dots, N\}$ in an odd transmission block, where the number of antennas equipped at the BS, relay R_1 and devices D_n are $A_0 = 4$, $A_1 = 4$, and $A_2 = 2$, respectively, and the PS factor $\lambda = 0.4$.

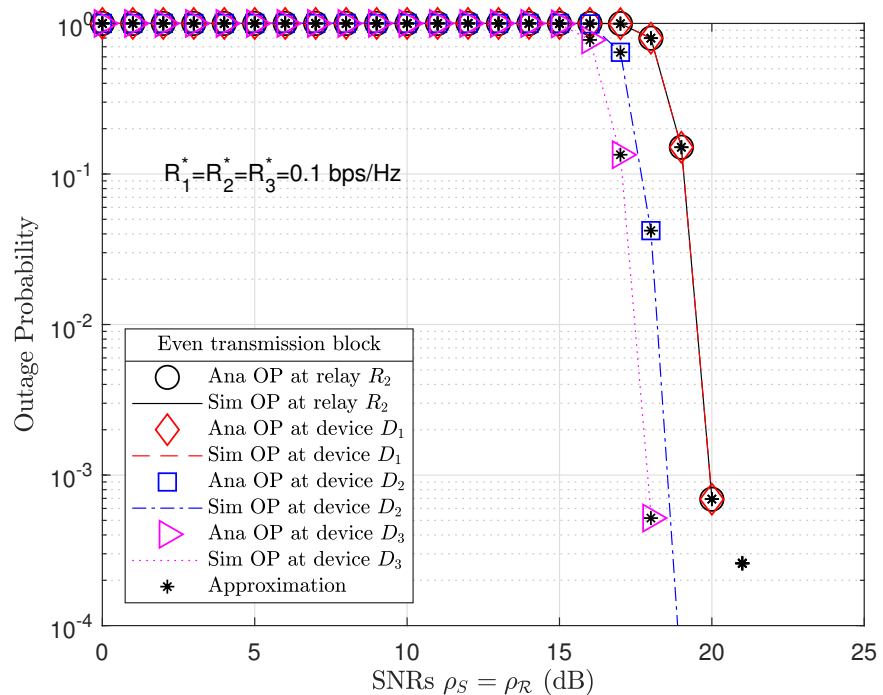


Figure 4. OP at relay R_2 and devices D_n for $n = \{1, \dots, N\}$ in an even transmission block, where the number of antennas equipped at the BS, relay R_2 and devices D_n are $A_0 = 4$, $A_1 = 16$, and $A_2 = 2$, respectively, and the PS factor $\lambda = 0.6$.

Figures 5 and 6 plot the system throughput performance at devices in odd and even transmission blocks, respectively. Even though device D_3 has the farthest distance from coupled relays ($d_3 = v_3 = 10$ m), device D_3 always achieved the best throughput performance compared to other devices. It is interesting that the system throughput results of relay R_1 and devices in odd transmission blocks (Figure 5) are similar to the system throughput results of relay R_2 and devices in even transmission blocks (Figure 6) at the same SNR.

To illustrate, we extract the investigated results from Matlab software. At a SNR range $\rho_S = \rho_R = \{15, \dots, 21\}$ dB, device throughput in odd and even transmission blocks achieved $TP^{(odd)} = \{0.0051, 0.0435, 0.1338, 0.2204, 0.279, 0.2983, 0.3\}$ and $TP^{(even)} = \{0.0011, 0.0261, 0.1287, 0.2169, 0.2849, 0.2999, 0.3\}$, respectively. We may observe that device throughput in odd transmission blocks outperformed device throughput in even transmission blocks at low SNRs, i.e., $\rho_S = \rho_R = \{15, \dots, 18\}$ dB. However, device throughput in even transmission blocks improved and outperformed device throughput in odd transmission blocks at high SNRs, i.e., $\rho_S = \rho_R = \{19, 20\}$ dB. Device throughput also tended toward their data rate thresholds, i.e., $R_1^* = R_2^* = R_3^* = 0.1$ b/s/Hz when the SNRs $\rho_S = \rho_R \rightarrow \infty$. As a result, system throughput in both odd and even transmission blocks $TP^{(odd)} = TP^{(even)} = R_1^* + R_2^* + R_3^* = 0.3$ b/s/Hz at high SNRs $\rho_S = \rho_R \geq 20$ dB. It is important to note that the PS factor in even transmission blocks ($\lambda = 0.6$) was greater than the PS factor in odd transmission blocks ($\lambda = 0.4$). Therefore, the relay R_1 in even transmission blocks harvested more energy than relay R_2 in odd transmission blocks. Certainly, even transmission blocks achieved better EE performance than odd transmission blocks.

Figure 7 plot the EE performance of odd even transmission blocks. We may observe that EE performance in the even transmission block with massive MIMO had a higher peak than the odd transmission block. The massive MIMO technique therefore not only provided greater throughput but also consumed less energy.

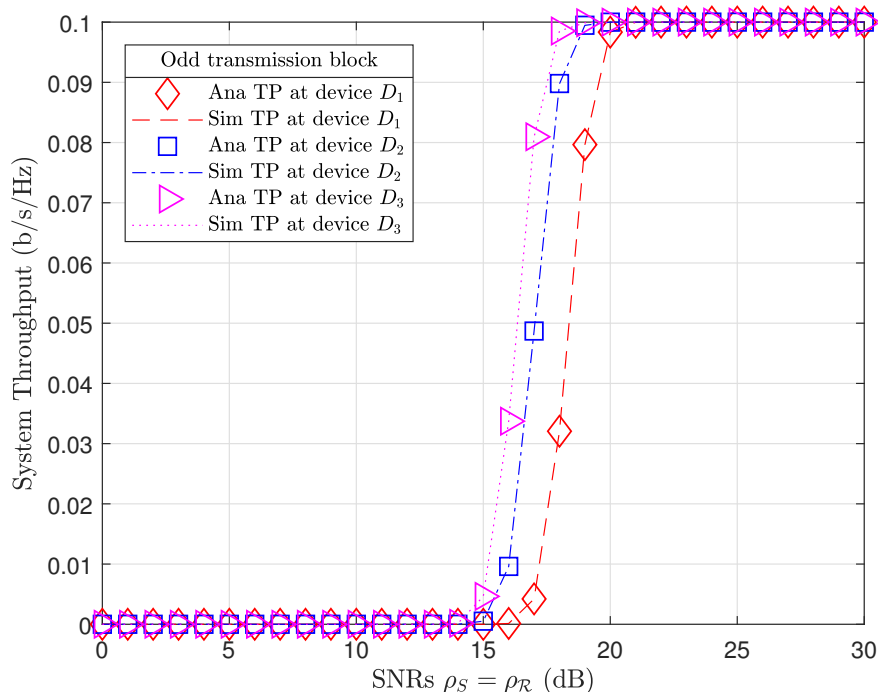


Figure 5. System throughput in odd transmission blocks.

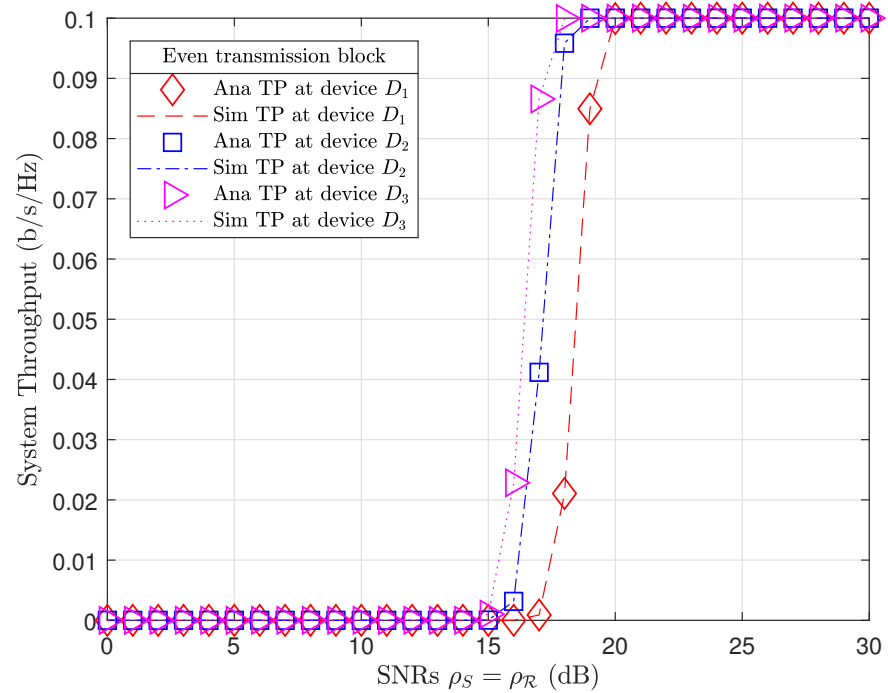


Figure 6. System throughput in even transmission blocks.

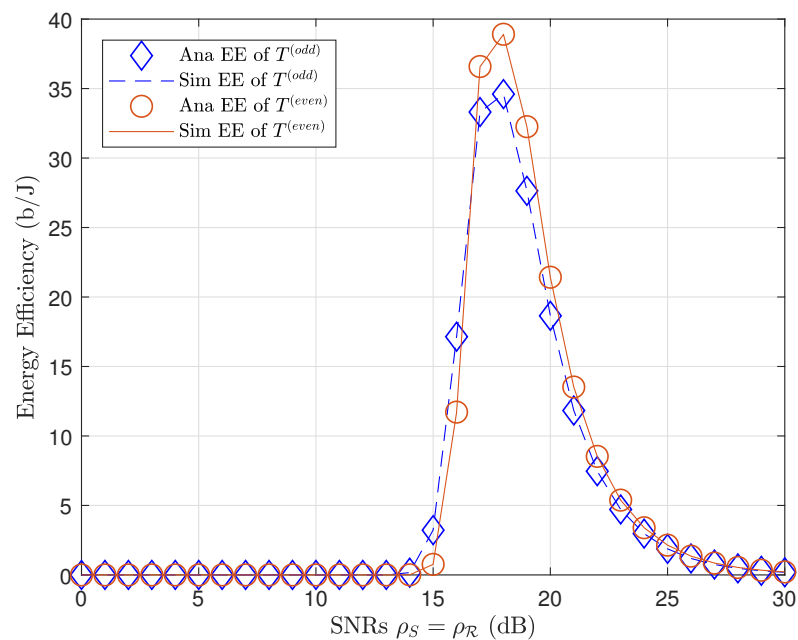


Figure 7. EE of a MIMO network (odd transmission block) compared to a massive MIMO network (even transmission block).

5. Conclusions

This paper proposes a design for a switchable coupled relay model to assist a massive MIMO-NOMA wireless network in serving multiple devices and extending a network's lifespan. A diagram of two transmission blocks illustrates signal propagation and EH processing. Propagation and formulations are analyzed. We derive the closed-form novel expressions for OP at the coupled relays and devices. The theoretical results show that the massive MIMO technique in combination with TAS and SWIPT protocols in an underlay

cooperative NOMA network provides higher throughput and consumes lower energy. The obtained results verify the massive MIMO technique as effective for 5G wireless networks. The present paper offers the potential for the practical application of a massive MIMO-NOMA network model assisted by switchable coupled relays, for example in a water environment where relays and devices are barely powered. Our massive MIMO-NOMA assisted by switchable coupled relays in combination with TAS and EH protocols can not only improve OP and system throughput performance but also extend the network's lifespan. Specifically, EH at the relay may be used to forward signals without consuming the relay's own energy. This is promising as a potential solution in extending a network's lifespan.

Author Contributions: These authors contributed equally to this work. All authors have read and agreed to the published version of the manuscript.

Funding: This research was funded by The Ministry of Education, Youth and Sports within the grant reg. No. SP2021/25 and partially within the Large Infrastructures for Research, Experimental Development, and Innovations project reg. No. LM2018140.

Institutional Review Board Statement: Not applicable.

Informed Consent Statement: Not applicable.

Data Availability Statement: Data was randomly generated when we were running program. There is no data to share.

Acknowledgments: We are especially grateful for our reviewers' comments and all the constructive suggestions that have helped us improve the quality and presentation of our manuscript.

Conflicts of Interest: The authors declare no conflict of interest. The funders had no role in the study's design, the collection, analysis and interpretation of data, writing of the manuscript, nor in the decision to publish the results.

Abbreviations

The following abbreviations are used in this manuscript:

5G	Fifth-Generation
AF	Amplify-and-Forward
AWGN	Adaptive White Gaussian Noise
BS	Base Station
CSI	Channel State Information
DF	Decode-and-Forward
EE	Energy Efficiency
EH	Energy Harvesting
FD	Full-Duplex
HD	Half-Duplex
IoTs	Internet of Things
MIMO	Multi-Input-Multi-Output
NOMA	Non-Orthogonal Multiple Access
OP	Outage Probability
PA	Power Allocation
PS	Power Splitting
QoS	Quality of Service
RF	Radio Frequency
SIC	Successive Interference Cancellation
SINR	Signal-to-Interference-plus-Noise Ratio
SISO	Single-Input-Single-Output
SNR	Signal-to-Noise Ratio
SWIPT	Simultaneously Wireless Information Power Transmit
TAS	Transmit Antennas Selection
TS	Time Switching
WIP	Wireless Information Power

Notations

The following notations are used in this manuscript:

N	$N \geq 1$	Number of devices
R_1, R_2		Coupled relays
d_{R_1}, d_{R_2}		Distances from BS to relays
\mathcal{R}	$\mathcal{R} = \{R_1, R_2\}$	Set of relays
D_n	$n \in N$	Devices
d_n	$n \in N$	Distances from relay R_1 to devices
v_n	$n \in N$	Distances from relay R_2 to devices
A_0, A_1, A_2	$A_0 > 1, A_1 > 1, A_2 > 1$	Number of antennas on BS, R_1 and R_2 , respectively
ω		Path-loss exponent factor
$\mathbf{H}_0, \mathbf{G}_0$		Pre-coding channel matrices from BS to R_1 and R_2
$h_0^{(a_0, a_1)}, g_0^{(a_0, a_1)}$	$a_0 \in A_0, a_1 \in A_1$	Channels from BS to R_1 and R_2
$\mathbf{H}_n, \mathbf{G}_n$		Pre-coding channel matrices from R_1 and R_2 to devices
θ	$\theta = \{odd, even\}$	binary value
$T^{(\theta)}$	$\theta = \{odd, even\}$	Odd/even transmission block
$h_n^{(a_0, a_1)}, g_n^{(a_0, a_1)}$	$n \in N, a_0 \in A_0, a_1 \in A_1$	Channels from relays R_1 and R_2 to devices
$T_1^{(\theta)}, T_2^{(\theta)}$		First/second time slot in odd/even transmission block
λ	$0 \leq \lambda \leq 1$	Power splitting factor
η	$0 \leq \eta \leq 1$	Collect factor
$P_S, P_{\mathcal{R}}$		Power domain on BS and relays
$\rho_S, \rho_{\mathcal{R}}$		SNR on BS and relays
α_i	$i \in N, \sum_i \alpha_i = 1, \alpha_1 < \dots < \alpha_N$	PA factors for devices
x_i	$i \in N$	Data of devices
$n_{\mathcal{R}}, n_n$	$n \in N$	AWGN at relays and devices
$\mathbf{Y}_{\mathcal{R}}^{(T_1^{(\theta)})}$	$\theta = \{odd, even\}, \mathcal{R} = \{R_1, R_2\}$	Received signals at relays
$\mathbf{Y}_n^{(T_2^{(\theta)})}$	$\theta = \{odd, even\}, n \in N$	Received signals at devices
R_i^*	$i \in N$	Devices' data rate thresholds
γ_i^*	$i \in N$	SINR thresholds
$\gamma_{\mathcal{R}-x_i}^{(T_1^{(\theta)})}$	$\theta = \{odd, even\}, \mathcal{R} = \{R_1, R_2\}, i \in N$	SINRs at relays decode symbol x_i
$\gamma_{n-x_i}^{(T_2^{(\theta)})}$	$\theta = \{odd, even\}, n \in N, i \in n$	SINRs at devices decode symbol x_i
$\mathbf{R}_{\mathcal{R}-x_i}^{(T_1^{(\theta)})}$	$\theta = \{odd, even\}, \mathcal{R} = \{R_1, R_2\}, i \in N$	Relays' instantaneous bit-rate thresholds
$\mathbf{R}_{n-x_i}^{(T_2^{(\theta)})}$	$\theta = \{odd, even\}, n \in N, i \in n$	Devices' instantaneous bit-rate thresholds
$E_{\mathcal{R}}^{(T_1^{(\theta)})}$	$\theta = \{odd, even\}, \mathcal{R} = \{R_1, R_2\}$	EH at relay R_1 or R_2 in odd/even transmission block
$OP_{\mathcal{R}}^{(T_1^{(\theta)})}$	$\theta = \{odd, even\}, \mathcal{R} = \{R_1, R_2\}$	OP at relays
$OP_n^{(\theta)}$	$\theta = \{odd, even\}, n \in N$	OP at devices
$TP^{(\theta)}$	$\theta = \{odd, even\}$	System throughput in odd/even transmission block
$EE^{(\theta)}$	$\theta = \{odd, even\}$	Energy efficiency in odd/even transmission block

Appendix A. Proof of Theorem 1

From (30), let

$$L_{\mathcal{R}-x_i}^{(T_1^{(\theta)})} = \Pr \left\{ \max_{[A_0 \times A_1]} \left\{ \mathbf{R}_{\mathcal{R}-x_i}^{(T_1^{(\theta)})} \right\} < R_i^* \right\} \underbrace{\prod_{k=N}^{i+1} \Pr \left\{ \max_{[A_0 \times A_1]} \left\{ \mathbf{R}_{\mathcal{R}-x_i}^{(T_1^{(\theta)})} \right\} \geq R_i^* \right\}}_{\text{for } i < N} \quad (\text{A1})$$

After some algebraic manipulation, we obtain

$$L_{\mathcal{R}-x_i}^{(T_1^{(\theta)})} = \Pr \left\{ \max_{[A_0 \times A_1]} \left\{ |\mathbf{H}_0|^2 \right\} < \frac{\gamma_i^*}{(1-\lambda)\beta_i\rho_S} \right\} \underbrace{\prod_{k=N}^{i+1} \Pr \left\{ \max_{[A_0 \times A_1]} \left\{ |\mathbf{H}_0|^2 \right\} \geq \frac{\gamma_i^*}{(1-\lambda)\beta_i\rho_S} \right\}}_{\text{for } i < N}. \quad (\text{A2})$$

From PDF expressions [23] (Equations (59) and (60)), we obtain

$$\begin{aligned}
 L_{\mathcal{R}-x_i}^{(T_1^{(\theta)})} &= \prod_{a_0=1}^{A_0} \prod_{a_1=1}^{A_1} \int_0^{\frac{\gamma_i^*}{(1-\lambda)\beta_i\rho_S}} \frac{\exp(-x/\sigma_{\mathcal{R}}^2)}{\sigma_{\mathcal{R}}^2} dx \underbrace{\prod_{k=N}^{i+1} \prod_{a_0}^{A_0} \prod_{a_1}^{A_1} \int_0^{\frac{\gamma_k^*}{(1-\lambda)\beta_k\rho_S}} \frac{\exp(-y/\sigma_{\mathcal{R}}^2)}{\sigma_{\mathcal{R}}^2} dy}_{i < N} \\
 &= \prod_{a_0=1}^{A_0} \prod_{a_1=1}^{A_1} \left(1 - \exp\left(-\frac{\gamma_i^*}{(1-\lambda)\beta_i\rho_S\sigma_{\mathcal{R}}^2}\right) \right) \underbrace{\prod_{k=N}^{i+1} \left(1 - \prod_{a_0}^{A_0} \prod_{a_1}^{A_1} \left(1 - \exp\left(-\frac{\gamma_k^*}{(1-\lambda)\beta_k\rho_S\sigma_{\mathcal{R}}^2}\right) \right) \right)}_{i < N}.
 \end{aligned} \tag{A3}$$

By substituting (A3) into (30), we obtain the expression of OP at coupled relays \mathcal{R} , as shown in (31).

From (34), we obtain

$$Q_i = \Pr \left\{ \max_{[A_0 \times A_1]} \left\{ \mathbf{R}_{\mathcal{R}-x_i}^{(T_1^{(\theta)})} \right\} \geq R_i^* \right\} = \Pr \left\{ \max_{[A_0 \times A_1]} \left\{ \gamma_{\mathcal{R}-x_i}^{(T_1^{(\theta)})} \right\} \geq \gamma_i^* \right\}. \tag{A4}$$

Appendix B. Proof of Remark 1

From [23] (Equation (71)), we obtain the CDF expression as follows:

$$F_{\max_{[A_0 \times A_1]} \left\{ \gamma_{\mathcal{R}-x_i}^{(T_1^{(\theta)})} \right\}}(\gamma) = \sum_{\psi=0}^{A_0 A_1} \frac{(-1)^\psi (A_0 A_1)!}{\psi! (A_0 A_1 - \psi)!} \exp\left(-\frac{\psi\gamma}{(1-\lambda)\left(\alpha_i - \gamma \sum_{j=1}^{i-1} \alpha_j\right)\rho_S\sigma_{\mathcal{R}}^2}\right), \tag{A5}$$

$$F_{\max_{[A_0 \times A_1]} \left\{ \gamma_{\mathcal{R}-x_i}^{(T_1^{(\theta)})} \right\}}(\gamma) = \sum_{\psi=0}^{A_0 A_1} \frac{(-1)^\psi (A_0 A_1)!}{\psi! (A_0 A_1 - \psi)!} \exp\left(-\frac{\psi\gamma}{(1-\lambda)\alpha_i\rho_S\sigma_{\mathcal{R}}^2}\right), \tag{A6}$$

where Expression (A5) is with $i > 1$ and $\gamma < \alpha_i / \sum_{j=1}^{i-1} \alpha_j$. If $\gamma \geq \alpha_i / \sum_{j=1}^{i-1} \alpha_j$, Expression (A5) refers to one. Expression (A6) is with $i = 1$.

By applying the CDF expressions as (A5) and (A6), we obtain

$$Q_i = 1 - F_{\max_{[A_0 \times A_1]} \left\{ \gamma_{\mathcal{R}-x_i}^{(T_1^{(\theta)})} \right\}}(\gamma_i^*) = 1 - \sum_{\psi=0}^{A_0 A_1} \frac{(-1)^\psi (A_0 A_1)!}{\psi! (A_0 A_1 - \psi)!} \exp\left(-\frac{\psi\gamma_i^*}{(1-\lambda)\beta_i\rho_S\sigma_{\mathcal{R}}^2}\right). \tag{A7}$$

By substituting (A7) into (34), we obtain OP at coupled relay, as shown in (35).

Appendix C. Proof of Theorem 2

From (36), we obtain

$$\begin{aligned}
OP_n^{(\theta)} = & \sum_{i=N}^n \left(\prod_{a_0}^{A_0} \prod_{a_1}^{A_1} \int_0^{\frac{\gamma_i^*}{(1-\lambda)\beta_i\rho_S}} \frac{\exp(-x/\sigma_{\mathcal{R}}^2)}{\sigma_{\mathcal{R}}^2} dx \prod_{k=N}^{i+1} \prod_{a_0}^{A_0} \prod_{a_1}^{A_1} \int_{\frac{\gamma_k^*}{(1-\lambda)\beta_k\rho_S}}^{\infty} \frac{\exp(-x/\sigma_{\mathcal{R}}^2)}{\sigma_{\mathcal{R}}^2} dx \right) \\
& + \sum_{i=N}^n \left(\prod_{a_1}^{A_1} \prod_{a_2}^{A_2} \int_0^{\frac{\gamma_i^*}{\beta_i\rho_{\mathcal{R}}}} \frac{\exp(-x/\sigma_n^2)}{\sigma_n^2} dx \prod_{k=N}^{i+1} \prod_{a_1}^{A_1} \prod_{a_2}^{A_2} \int_{\frac{\gamma_k^*}{\beta_k\rho_{\mathcal{R}}}}^{\infty} \frac{\exp(-x/\sigma_n^2)}{\sigma_n^2} dx \right. \\
& \quad \left. \times \prod_{i=N}^n \prod_{a_0}^{A_0} \prod_{a_1}^{A_1} \int_{\frac{\gamma_i^*}{(1-\lambda)\beta_i\rho_S}}^{\infty} \frac{\exp(-x/\sigma_{\mathcal{R}}^2)}{\sigma_{\mathcal{R}}^2} dx \right)
\end{aligned} \tag{A8}$$

Expression (A8) can be solved and obtained in closed-form, as shown in (37).

Appendix D. Proof of Remark 2

From (38), we obtain

$$OP_n^{(\theta)} = 1 - \prod_{i=N}^n \left(1 - F_{\max_{[A_0 \times A_1]} \left\{ \gamma_{\mathcal{R}-x_i}^{(T_1^{(\theta)})} \right\}}(\gamma_i^*) \right) \left(1 - F_{\max_{[A_1 \times A_2]} \left\{ \gamma_{n-x_i}^{(T_2^{(\theta)})} \right\}}(\gamma_i^*) \right), \tag{A9}$$

where $F_{\max_{[A_0 \times A_1]} \left\{ \gamma_{\mathcal{R}-x_i}^{(T_1^{(\theta)})} \right\}}(\gamma)$ is given by (A5) or (A6) and $F_{\max_{[A_1 \times A_2]} \left\{ \gamma_{n-x_i}^{(T_2^{(\theta)})} \right\}}(\gamma)$ is given by

$$F_{\max_{[A_1 \times A_2]} \left\{ \gamma_{n-x_i}^{(T_2^{(\theta)})} \right\}}(\gamma) = \sum_{\mu=0}^{A_1 A_2} \frac{(-1)^\mu (A_0 A_1)!}{\mu! (A_0 A_1 - \mu)!} \exp \left(- \frac{\mu \gamma}{\left(\alpha_i - \gamma \sum_{j=1}^{i-1} \alpha_j \right) \rho_{\mathcal{R}} \sigma_n^2} \right), \tag{A10}$$

$$F_{\max_{[A_1 \times A_2]} \left\{ \gamma_{n-x_i}^{(T_2^{(\theta)})} \right\}}(\gamma) = \sum_{\mu=0}^{A_1 A_2} \frac{(-1)^\mu (A_1 A_2)!}{\mu! (A_1 A_2 - \mu)!} \exp \left(- \frac{\mu \gamma}{\alpha_i \rho_{\mathcal{R}} \sigma_n^2} \right), \tag{A11}$$

where Expression (A10) is with $i > 1$ and $0 \leq \gamma < \alpha_i / \sum_{j=1}^{i-1} \alpha_j$ and Expression (A11) is with $i = 1$ and $\gamma \geq 0$.

By substituting Expressions (A5), (A6), (A10), and (A11) into Expression (A9), we obtain OP at devices D_n in closed-form, as shown in (39).

References

- Zhang, S.; Wu, Q.; Xu, S.; Li, G. Fundamental green tradeoffs: Progresses challenges and impacts on 5G networks. *IEEE Commun. Surv. Tutor.* **2017**, *19*, 33–56. [\[CrossRef\]](#)
- Zhu, C.; Leung, V.C.M.; Shu, L.; Ngai, E.C.-H. Green Internet of Things for Smart World. *IEEE Access* **2015**, *3*, 2151–2162 [\[CrossRef\]](#)
- Saito, Y.; Kishiyama, Y.; Benjebbour, A.; Nakamura, T.; Li, A.; Higuchi, K. Non-Orthogonal Multiple Access (NOMA) for Cellular Future Radio Access. In Proceedings of the 2013 IEEE 77th Vehicular Technology Conference (VTC Spring), Dresden, Germany, 2–5 June 2013.
- Higuchi, K.; Benjebbour, A. Non-orthogonal Multiple Access (NOMA) with Successive Interference Cancellation for Future Radio Access. *IEICE Trans. Commun.* **2015**, *98*, 403–414. [\[CrossRef\]](#)

5. Li, Q.C.; Niu, H.; Papathanassiou, A.T.; Wu, G. 5G Network Capacity: Key Elements and Technologies. *IEEE Veh. Technol. Mag.* **2014**, *9*, 71–78. [[CrossRef](#)]
6. Islam, S.M.R.; Avazov, N.; Dobre, O.A.; Kwak, K.-S. Power-Domain Non-Orthogonal Multiple Access (NOMA) in 5G Systems: Potentials and Challenges. *IEEE Commun. Surv. Tutor.* **2017**, *19*, 721–742. [[CrossRef](#)]
7. Ding, Z.; Yang, Z.; Fan, P.; Poor, H.V. On the Performance of Non-Orthogonal Multiple Access in 5G Systems with Randomly Deployed Users. *IEEE Signal Process. Lett.* **2014**, *21*, 1501–1505. [[CrossRef](#)]
8. Timotheou, S.; Krikidis, I. Fairness for Non-Orthogonal Multiple Access in 5G Systems. *IEEE Signal Process. Lett.* **2015**, *22*, 1647–1651. [[CrossRef](#)]
9. Fang, F.; Zhang, H.; Cheng, J.; Leung, V.C.M. Energy-Efficient Resource Allocation for Downlink Non-Orthogonal Multiple Access Network. *IEEE Trans. Commun.* **2016**, *64*, 3722–3732. [[CrossRef](#)]
10. Seddik, K.; Sadek, A.; Su, W.; Liu, K. Outage analysis and optimal power allocation for multinode relay networks. *IEEE Signal Process. Lett.* **2007**, *14*, 377–380. [[CrossRef](#)]
11. Takahashi, M.; Kawamoto, Y.; Kato, N.; Miura, A.; Toyoshima, M. Adaptive Power Resource Allocation with Multi-Beam Directivity Control in High-Throughput Satellite Communication Systems. *IEEE Wirel. Commun. Lett.* **2019**, *8*, 1248–1251. [[CrossRef](#)]
12. Tran, T.-N.; Voznak, M. Multi-Points Cooperative Relay in NOMA System with N-1 DF Relaying Nodes in HD/FD Mode for N User Equipments with Energy Harvesting. *Electronics* **2019**, *8*, 167. [[CrossRef](#)]
13. Tran, T.-N.; Voznak, M. HD/FD and DF/AF with Fixed-Gain or Variable-Gain Protocol Switching Mechanism over Cooperative NOMA for Green-Wireless Networks. *Sensors* **2019**, *19*, 1845. [[CrossRef](#)]
14. Kim, J.-B.; Lee, I.-H. Capacity Analysis of Cooperative Relaying Systems Using Non-Orthogonal Multiple Access. *IEEE Commun. Lett.* **2015**, *19*, 1949–1952. [[CrossRef](#)]
15. Pei, L.; Yang, Z.; Pan, C.; Huang, W.; Chen, M.; Elkashlan, M.; Nallanathan, A. Energy-Efficient D2D Communications Underlying NOMA-Based Networks with Energy Harvesting. *IEEE Commun. Lett.* **2018**, *22*, 914–917. [[CrossRef](#)]
16. Sreng, V.; Yanikomeroglu, H.; Falconer, D. Relay selection strategies in cellular networks with peer-to-peer relaying. In Proceedings of the 2003 IEEE 58th Vehicular Technology Conference, VTC 2003-Fall (IEEE Cat. No. 03CH37484), Orlando, FL, USA, 6–9 October 2003.
17. Jing, Y.; Jafarkhani, H. Single and multiple relay selection networks and their achievable diversity orders. *IEEE Trans. Wirel. Commun.* **2009**, *8*, 1414–1423. [[CrossRef](#)]
18. Lee, S.; Da Costa, D.B.; Vien, Q.-T.; Duong, T.Q.; De Sousa, R.T. Non-orthogonal multiple access schemes with partial relay selection. *IET Commun.* **2017**, *11*, 846–854. [[CrossRef](#)]
19. Liu, Y.; Wang, L.; Duy, T.T.; Elkashlan, M.; Duong, T.Q. Relay Selection for Security Enhancement in Cognitive Relay Networks. *IEEE Wirel. Commun. Lett.* **2015**, *4*, 46–49. [[CrossRef](#)]
20. Yang, S.; Hanzo, L. Fifty Years of MIMO Detection: The Road to Large-Scale MIMOs. *IEEE Commun. Surv. Tutor.* **2015**, *17*, 1941–1988. [[CrossRef](#)]
21. Shirvanimoghaddam, M.; Dohler, M.; Johnson, S.J. Massive Non-Orthogonal Multiple Access for Cellular IoT: Potentials and Limitations. *IEEE Commun. Mag.* **2017**, *55*, 55–61. [[CrossRef](#)]
22. Chen, C.; Zhong, W.-D.; Yang, H.; Du, P. On the Performance of MIMO-NOMA-Based Visible Light Communication Systems. *IEEE Photonics Technol. Lett.* **2018**, *30*, 307–310. [[CrossRef](#)]
23. Tran, T.-N.; Voznak, M. On secure system performance over SISO, MISO and MIMO-NOMA wireless networks equipped a multiple antenna based on TAS protocol. *EURASIP J. Wirel. Commun. Netw.* **2020**, *2020*, 1–22. [[CrossRef](#)]
24. Lei, H.; Zhang, J.; Park, K.H.; Xu, P.; Ansari, I.S.; Pan, G.; Alomair, B.; Alouini, M.-S. On Secure NOMA Systems with Transmit Antenna Selection networks. *IEEE Access* **2017**, *5*, 17450–17464. [[CrossRef](#)]
25. Liu, Y.; Ding, Z.; Elkashlan, M.; Poor, H. Cooperative non-orthogonal multiple access in 5G systems with SWIPT. In Proceedings of the 2015 23rd European Signal Process. Conf. (EUSIPCO), Nice, France, 31 August–4 September 2015.
26. Lu, X.; Wang, P.; Niyato, D.; Kim, D.I.; Han, Z. Wireless Networks with RF Energy Harvesting: A Contemporary Survey. *IEEE Commun. Surv. Tutor.* **2014**, *17*, 757–789. [[CrossRef](#)]
27. Hadzi-Velkov, Z.; Nikoloska, I.; Karagiannidis, G.K.; Duong, T.Q. Wireless Networks with Energy Harvesting and Power Transfer: Joint Power and Time Allocation. *IEEE Signal Process. Lett.* **2015**, *23*, 50–54. [[CrossRef](#)]
28. Chen, X.; Yuen, C.; Zhang, Z. Wireless Energy and Information Transfer Tradeoff for Limited-Feedback Multiantenna Systems with Energy Beamforming. *IEEE Trans. Veh. Technol.* **2013**, *63*, 407–412. [[CrossRef](#)]
29. Yang, Z.; Ding, Z.; Fan, P.; Al-Dhahir, N. The Impact of Power Allocation on Cooperative Non-orthogonal Multiple Access Networks with SWIPT. *IEEE Trans. Wirel. Commun.* **2017**, *16*, 4332–4343. [[CrossRef](#)]
30. Ye, Y.; Li, Y.; Wang, D.; Lu, G. Power splitting protocol design for the cooperative NOMA with SWIPT. In Proceedings of the 2017 IEEE International Conference on Communications (ICC), Paris, France, 21–25 May 2017.
31. Perera, T.D.P.; Jayakody, D.N.K. Analysis of time-switching and power-splitting protocols in wireless-powered cooperative communication system. *Phys. Commun.* **2018**, *31*, 141–151. [[CrossRef](#)]
32. Esmail, H.; Qasem, Z.; Sun, H.; Qi, J.; Wang, J.; Gu, Y. Wireless information and power transfer for underwater acoustic time-reversed NOMA. *IET Commun.* **2020**, *14*, 3394–3403. [[CrossRef](#)]

-
33. Ngo, H.Q.; Duong, T.Q.; Larsson, E.G. Uplink performance analysis of multicell MU-MIMO with zero-forcing receivers and perfect CSI. In Proceedings of the 2011 IEEE Swedish Communication Technologies Workshop (Swe-CTW), Stockholm, Sweden, 19–21 October 2011; pp. 40–45.
 34. Lorincz, J.; Chiaraviglio, L.; Cuomo, F. A measurement study of short-time cell outages in mobile cellular networks. *Comput. Commun.* **2016**, *79*, 92–102. [[CrossRef](#)]
 35. Wei, Z.; Yuan, J.; Ng, D.W.K.; Elkashlan, M.; Ding, Z. A survey of downlink non-orthogonal multiple access for 5G wireless communication networks. *ZTE Commun.* **2016**, *14*, 17–25.